INTERNATIONAL JOURNAL FOR NUMERICAL METHODS IN FLUIDS, VOL. 26, 581–603 (1998)
Int. J. Numer. Meth. Fluids **26**: 581–603 (1998)

TWO- AND THREE-DIMENSIONAL LAMINAR FLOWS BETWEEN DISKS CO-ROTATING IN A FIXED CYLINDRICAL ENCLOSURE

IMMACULADA IGLESIAS[a] AND JOSEPH A.C. HUMPHREY[b,*]

[a] *Departamento de Ingeniería Mecánica de Fluidos, Escuela Politécnica Superior, Universidad Carlos III de Madrid, Madrid, Spain*
[b] *Department of Mechanical Engineering, Bucknell University, Lewisburg, PA 17837, U.S.A.*

SUMMARY

A numerical investigation is performed for the constant property laminar flow of air in the space between a pair of disks clamped co-axially on a central hub and co-rotating in a stationary cylindrical enclosure. Both two- and three-dimensional flow conditions are examined in relation to the interdisk spacing, H, and the disk angular velocity, Ω. Two interdisk spacings are considered, corresponding to aspect ratios $\Gamma = 0.186$ and 0.279 (with $\Gamma = H/(R_2 + a - R)$, where R_2 is the disk radius, a is the disk rim–enclosure wall clearance, and R is the hub radius). A range of rotational speeds encompassing the transition from axisymmetric two-dimensional steady flow to non-axisymmetric three-dimensional unsteady flow is considered for various values of the Reynolds number, Re (with $Re = \Omega R_2^2/v$, where v is the kinematic viscosity of air). Axisymmetric calculations are first performed for both aspect ratios in the range $3858 \leq Re \leq 23\,150$. Fully three-dimensional calculations are then performed for the configuration with $\Gamma = 0.186$ and $Re = 23\,150$, and for the configuration with $\Gamma = 0.279$ and $Re = 7715$, 15 430 and 23 150. The axisymmetric calculations performed with $\Gamma = 0.186$ confirm many known features of the flow, including the transition from a steady flow to an oscillatory periodic regime. This occurs at $\approx Re = 23\,150$ for a configuration with $a/H = 0$, and at $\approx Re = 14\,670$ for one with $a/H = 0.28$ and a finite disk thickness ($b/H = 0.2$). Three-dimensional calculations performed for $\Gamma = 0.186$ with $a/H = 0$ and $Re = 23\,150$ reveal a circumferentially periodic flow pattern with eight foci of intensified axial component of vorticity. The axisymmetric calculations performed with $\Gamma = 0.279$ and $Re > 7715$ yield a novel, non-unique steady solution for the velocity field that is asymmetric with respect to the interdisk mid-plane. No experimental verification of this finding exists to date, but similar situations are known to arise in the context of anomalous modes of the Taylor–Couette flow. Relaxing the axisymmetry constraint allows this flow to evolve to an oscillatory three-dimensional regime of increasing irregularity with increasing rotational speed. In this case, the number of foci of intensified axial vorticity varies with time, ranging from six at $Re = 7715$ to between six and eight at $Re = 23\,150$. © 1998 John Wiley & Sons, Ltd.

KEY WORDS: rotating co-rotating disks; disk drives; laminar flow; numerical calculations

1. INTRODUCTION

1.1. The problem of interest and prior work

The flow configuration of interest is shown in Figure 1. It consists of a pair of disks clamped

* Correspondence to: Department of Mechanical Engineering, Bucknell University, Lewisburg, PA 17837, U.S.A.

CCC 0271–2091/98/050581–23$17.50

Received 26 August 1996
Revised 28 April 1997

co-axially on a central hub that rotates in a stationary cylindrical enclosure. Small aspect ratios are considered since they are especially relevant to industrial and technical applications. The constant-property laminar flow of air between the two co-rotating disks is calculated using a second-order-accurate (in space and time) numerical procedure that solves discretized forms of mass and momentum conservation equations subject to appropriate initial and boundary conditions. The flow configuration is investigated in relation to two parameters: the dimensionless aspect ratio, Γ, and the Reynolds number, *Re*, defined above. The aspect ratios considered are 0.186 and 0.279, and the values of the Reynolds number range from 3858 to 23 150, corresponding to rotation rates ranging from 50 to 300 rpm.

The configuration of coaxial disks co-rotating in a cylindrical enclosure provides a useful model for investigating flows in the hard disk drives used as data storage devices in computers. A better understanding of the complex unsteady flows that arise in disk storage devices is essential for their improved design and repeatable operation. A disk storage system consists of a stack of equidistant, centrally clamped disks co-rotating in a non-axisymmetric enclosure. The electronic data are distributed along micron-sized circular tracks on the disk surfaces. Data transfer to and from the disks is accomplished by means of magnetic heads suspended at sub-micron distances from the rotating disk surfaces by rigid supports. Very small dimensions and high speeds of rotation are required to obtain high data transfer rates and, currently, important issues include minimizing track misregistration and viscous dissipation of mechani-

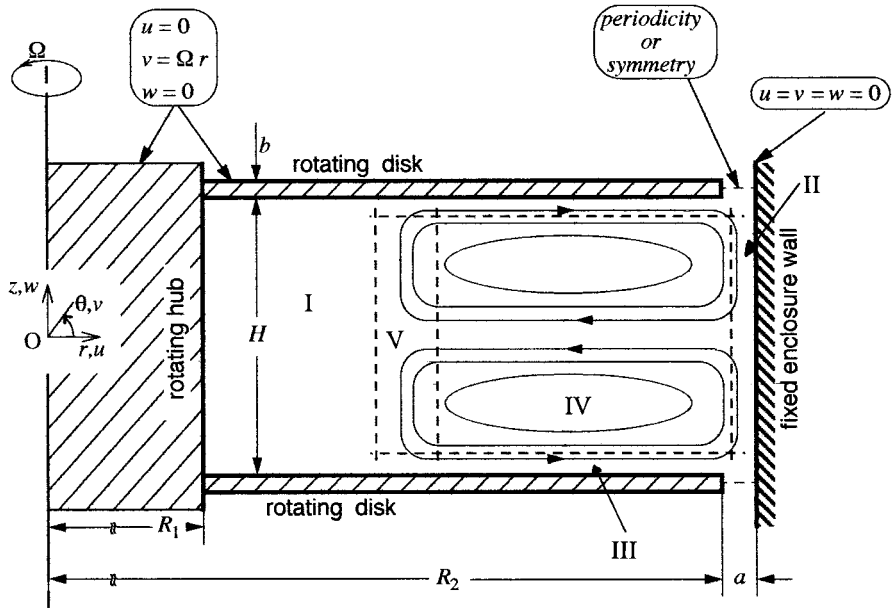

Figure 1. Sketch showing the flow configuration of interest. This consists of a pair of disks clamped on a central hub, co-rotating in a fixed cylindrical enclosure. The basic flow regions (I–V) induced in the interdisk space are sketched in accordance with previous studies [4]. In the bulk of the calculations, $R_1 = 56.4$ mm, $R_2 = 107.7$ mm, $H = 9.53$ mm or 14.3 mm, $a = 0$, and $b = 0$. Selective calculations have been performed with $R_1 = 56.4$ mm, $R_2 = 105.0$ mm, $H = 9.53$ mm, $a = 2.7$ mm, and $b = 1.91$ mm. The latter values correspond exactly to an experimental configuration used in other studies [4,6,7,20].

cal energy into heat. As the sizes of modern drives decrease, the associated flows include both laminar and turbulent regimes because the disk angular velocity, Ω, varies linearly and R_2 (the disk radius) varies quadratically in the definition of the Reynolds number. In this regard, the investigation of an idealized unobstructed laminar flow system is a very helpful first step.

As discussed below, the present unobstructed configuration has been previously studied by various authors using experimental, numerical and analytical approaches. With reference to Figure 1, the basic time-averaged flow can be summarized as follows. Fluid near the rotating disks is dragged circumferentially due to viscous shear. Similarly, viscous shear at the fixed enclosure wall decelerates the circumferential component of motion in its vicinity. The radial pressure gradient induced by this slower circumferential motion is unable to produce the necessary centripetal acceleration that would maintain the flow in purely circumferential motion. From the point of view of a rotating frame of reference, the pressure gradient force acting radially inward is unable to balance the centrifugal force acting radially outward on fluid near the rotating disks. As a result, boundary (or Ekman) layers containing fluid that has both radial and circumferential components of motion develop on the disks. The fluid driven outward in the Ekman layers by the imbalance in radial forces is replaced by an axial flow from the core that can only be maintained through the establishment of an inward-directed radial flow. Near the fixed enclosure, the fluid thrown radially outward in the Ekman layers is redirected in the axial direction along the enclosure wall, and then radially inward, back into the core. Combined with the circumferential spin, this motion produces a pair of toroidal vortices in the interdisk space. The bulk of this study is concerned with the stability of this toroidal vortex pair. In practical applications, a small radial clearance exists between the rim of a rotating disk and the stationary enclosure. This radial gap is neglected in most of the present calculations, but the effect of the simplification on the computed flow fields is assessed.

Early experimental studies of flows in disk drives were performed by Lennemann [1] and Kaneko *et al.* [2], using flow visualization in configurations which were geometrically and dynamically similar to the present one. These authors observed a region of laminar flow near the hub, separated from a region of turbulent flow near the enclosure wall, with a polygonally shaped boundary between the two rotating at about 80% of the disk angular velocity. Subsequently, Abrahamson *et al.* [3] observed three similar regions of flow that they referred to as an 'inner' region in solid body rotation near the hub, an 'outer' region containing foci of intensified axial component of vorticity, and a boundary layer along the enclosure wall. The foci of vorticity were distributed periodically in the circumferential direction and rotated at about 75% of the disk angular velocity. Their number was observed to decrease with increased disk spacing or rotation velocity.

Laser–Doppler velocimeter (LDV) measurements made by Schuler *et al.* [4,20], Tzeng and Humphrey [5] and Humphrey *et al.* [6] reveal maxima in the radial profiles of the root mean square of the circumferential velocity component. The maxima were attributed to large oscillations produced by the periodic passage of the vortical foci. Analysis of the data in Humphrey *et al.* [6] suggests that the number of foci is even and decreases in a stepwise manner with increasing Reynolds number. For the special case of axisymmetric steady motion, Schuler *et al.* [4] present a theoretical analysis based on scaling considerations. With reference to Figure 1, the analysis shows that fluid motion in the interdisk space can be divided into five regions: (i) a region essentially in solid body rotation near the hub; (ii) a region of strongly sheared fluid near the fixed enclosure wall; (iii) a pair of Ekman layers, developing on the facing surfaces of the two disks; (iv) a core region of potential flow, characterized by moderate velocity gradients in the radial direction and negligible gradients in

the axial direction; and (v) an axially aligned detached shear layer (or Stewartson layer) that allows the transition between the three-dimensional motion in the potential core and the region of flow in solid body rotation.

The flow visualization and LDV measurements of Humphrey and Gor [7] confirm the scaling results of Schuler *et al.* [4] for the thickness and radial location of the detached shear layer. They also found that, beyond a critical value of the Reynolds number which depends on the interdisk spacing, the detached shear layer oscillates axially in the cross-stream (r–z) plane. The unsteadiness of the detached shear layer and the fluid around it is believed to originate at the enclosure sidewall, where the streams in the turning Ekman layers collide. Humphrey and Gor [7] postulated a connection between the periodic oscillations of the cross-stream flow and the circumferentially distributed vortical foci. This was subsequently verified by the numerical calculations of Humphrey *et al.* [6]. In both of these studies, the onset of unsteadiness is associated with a two- to three-dimensional transition in flow structure. Experimental measurements suggest that this occurs at approximately $Re \simeq 4730$ for $\Gamma = 0.186$, and $Re \simeq 4070$ for $\Gamma = 0.279$.

A theoretical expression for predicting the torque required to spin one or more disks in a fixed cylindrical enclosure, with or without interdisk obstructions, was derived by Humphrey *et al.* [8]. The expression correlates the available data to within 5–20%, depending on the configuration geometry and Reynolds number. Using numerical calculation, these authors also show the extent to which imposing a radial ventilation condition (blowing or suction) affects the stability of the interdisk flow and the associated power dissipation.

Other numerical investigations of unobstructed flows between co-rotating disks in cylindrical enclosures include the axisymmetric steady flow cases investigated by Chang *et al.* [9] and Tzeng and Fromm [10] in the laminar regime, and by Chang *et al.* [11] and Tzeng and Humphrey [5] in the turbulent regime. However, the most interesting numerical results correspond to the two- and three-dimensional unsteady flow cases calculated by Humphrey *et al.* [6] for the experimental conditions investigated by Schuler *et al.* [4]. This study covers a range of Reynolds numbers in which the flow is laminar but experiences a transition from steady axisymmetric motion to unsteady three-dimensional motion at approximately $Re = 22\,000$. The three-dimensional calculations show that the pair of toroidal vortices in the interdisk space acquire a sinuous (slinky-like) shape that varies with time and position in the circumferential direction. The result is that the symmetry of the motion about the interdisk mid-plane is broken by alternating periodic crossings of this plane by the distorted toroidal vortices, with the speed of the wave driving this motion being smaller than the disk speed of rotation, as observed experimentally. A contour map of the axial vorticity component projected on the interdisk mid-plane reveals an even integer number of circumferentially periodic foci. A model for the unsteady periodic three-dimensional flow is proposed in which the presence of the vortical foci is intimately connected to the variation of the circumferential velocity component in the (r–θ) plane that, in turn, is linked to the circumferential variation of the axial velocity component. The model establishes a definite connection between the cross-stream flow and the circumferentially distributed foci of axial vorticity, as had been postulated by Humphrey and Gor [7]. The interpretation of the three-dimensional calculations, together with experimental data from previous works, led Humphrey *et al.* [6] to suggest that the transition from a steady axisymmetric flow to an unsteady three-dimensional wavy flow may be due to a secondary shear instability of the type associated with Dean vortex flow [12].

1.2. Objectives of this study

The main objective of this study is to calculate and interpret the unobstructed rotating disk flow configurations investigated by Humphrey and Gor [7] and Humphrey *et al.* [6] using a more refined three-dimensional grid and a more systematic approach than presented in the latter reference. These authors examined geometries corresponding to the present ones, except that the disk rim–enclosure wall gap was $a/H = 0.28$, where a is the disk rim–enclosure wall clearance and H is the interdisk spacing, and in the experiment, the disk thickness was $b/H = 0.20$. In the bulk of the present work, $a/H = 0$ and $b/H = 0$. Nevertheless, a case corresponding to the experimental values of a/H and b/H is examined for the influence on the interdisk flow resulting from the boundary conditions imposed in the gap. A related objective is to compare the experimentally determined and numerically calculated dependence of the number and distribution of vortical foci as a function of the interdisk spacing, Γ, and the disk speed of rotation, Re. Both two-dimensional (axisymmetric) and three-dimensional flow conditions are examined in this study.

2. NUMERICAL PROCEDURE

2.1. Conservation equations and boundary conditions

The mass and momentum conservation equations for a constant-property flow, written for the fixed cylindrical co-ordinate system shown in Figure 1, with u, v and w being the radial, circumferential, and axial components of the velocity vector, are given by:

$$\text{mass:} \quad \frac{1}{r}\frac{\partial(ru)}{\partial r} + \frac{1}{r}\frac{\partial v}{\partial \theta} + \frac{\partial w}{\partial z} = 0, \tag{1}$$

$$r\text{-momentum:} \quad \frac{\partial u}{\partial t} + u\frac{\partial u}{\partial r} + \frac{v}{r}\frac{\partial u}{\partial \theta} + w\frac{\partial u}{\partial z} - \frac{v^2}{r} = -\frac{1}{\rho}\frac{\partial p}{\partial r} + \nu\left(\nabla^2 u - \frac{2}{r^2}\frac{\partial v}{\partial \theta} - \frac{u}{r^2}\right), \tag{2}$$

$$\theta\text{-momentum:} \quad \frac{\partial v}{\partial t} + u\frac{\partial v}{\partial r} + \frac{v}{r}\frac{\partial v}{\partial \theta} + w\frac{\partial v}{\partial z} + \frac{uv}{r} = -\frac{1}{\rho r}\frac{\partial p}{\partial \theta} + \nu\left(\nabla^2 v + \frac{2}{r^2}\frac{\partial u}{\partial \theta} - \frac{v}{r^2}\right), \tag{3}$$

$$z\text{-momentum:} \quad \frac{\partial w}{\partial t} + u\frac{\partial w}{\partial r} + \frac{v}{r}\frac{\partial w}{\partial \theta} + w\frac{\partial w}{\partial z} = -\frac{1}{\rho}\frac{\partial p}{\partial z} + \nu\nabla^2 w, \tag{4}$$

with

$$\nabla^2 = \frac{1}{r}\frac{\partial}{\partial r}\left(r\frac{\partial}{\partial r}\right) + \frac{1}{r^2}\frac{\partial^2}{\partial \theta^2} + \frac{\partial^2}{\partial z^2}. \tag{5}$$

For the case of axisymmetric two-dimensional flow, Equations (1)–(5) are simplified by setting $\partial/\partial\theta = 0$. Noting that the origin for the z-co-ordinate is located on the interdisk mid-plane, the boundary conditions are:

(a) Rotating disk surfaces: $u = w = 0$ and $v = \Omega r$.
(b) Rotating hub surface: $u = w = 0$ and $v = \Omega R_1$ (where R_1 is the hub radius).
(c) Enclosure wall surface: $u = v = w = 0$.
(d) Disk rim–enclosure wall gap: Two types of boundary conditions are explored, symmetry and periodicity. Both conditions are compatible with the assumption of an infinite stack of disks. Symmetry is imposed by setting $\partial u/\partial z = \partial v/\partial z = w = 0$ at $z = \pm(H + b)/2$ in the gap. Periodicity is imposed by requiring $\{\boldsymbol{u}, p\}_{\mathbf{z}=(\mathrm{H}+\mathrm{b})/2} = \{\boldsymbol{u}, p\}_{\mathbf{z}=-(\mathrm{H}+\mathrm{b})/2}$, where $\boldsymbol{u}$ is the velocity vector and p is the pressure including the gravitational body force terms.

(e) In the three-dimensional calculations, the boundary condition in the circumferential direction, imposed by the geometry of the problem, is periodicity, with a period of 2π; i.e. $\{\boldsymbol{u}, p\}_{\theta=0} = \{\boldsymbol{u}, p\}_{\theta=2\pi}$. In the axisymmetric calculations there is no circumferential variation of the velocity, therefore $\partial \boldsymbol{u}/\partial\theta = 0$ and the simplified equations are solved for only one $(r-z)$ plane.

For each Γ, the first axisymmetric flow calculation at the lowest Reynolds number is started from rest. Subsequent axisymmetric calculations for a given Γ at increasingly higher values of the Reynolds number are started from an instantaneous converged solution of the flow field obtained at the immediately preceding (lower) Reynolds number. Similarly, the first three-dimensional flow calculations, with $\Gamma = 0.186$ and $Re = 23\,150$ and with $\Gamma = 0.279$ and $Re = 15\,430$, respectively, are started from rest. The higher and lower Reynolds number cases for $\Gamma = 0.279$ are started from an instantaneous converged three-dimensional solution of the intermediate case with $Re = 15\,430$.

Calculations are performed in the physical space using the properties of air at 25°C, where $\rho = 1.177$ kg m^{-3} and $\mu = 1.853 \times 10^{-5}$ kg ms^{-1}. However, for the purpose of presenting results, the following non-dimensional variables are defined:

$$U = \frac{u}{\Omega R_2}, \qquad V = \frac{v}{\Omega R_2}, \qquad W = \frac{w}{\Omega R_2}, \tag{6}$$

$$R = \frac{r - R_1}{R_2 - R_1}, \qquad Z = \frac{z}{H}, \tag{7}$$

$$\omega_\theta = \frac{1}{\Omega}\left(\frac{\partial u}{\partial z} - \frac{\partial w}{\partial r}\right), \qquad \omega_z = \frac{1}{\Omega r}\left(\frac{\partial (rv)}{\partial r} - \frac{\partial u}{\partial \theta}\right), \tag{8}$$

$$\frac{\partial \psi}{\partial z} = \frac{ru}{\Omega R_2^3}, \qquad \frac{\partial \psi}{\partial r} = -\frac{rw}{\Omega R_2^3}. \tag{9}$$

2.2. Summary of the solution algorithm

Calculations of the flow are performed using the CUTEFLOWS numerical procedure [6]. This program calculates unsteady, three-dimensional, constant-property flows in Cartesian or cylindrical co-ordinates. The algorithm is based on a finite difference representation of the conservation equations, which is explicit and second-order-accurate in space and time. A detailed exposition of the finite differencing practices and solution methodology of the numerical algorithm is available in Reference [13], including rigorous tests pertinent to the present flow. A very brief summary of the algorithm follows.

The finite difference equations are derived using a staggered grid control volume formulation of the conservation equations in terms of the primitive variables of velocity and pressure. The continuity equation is integrated over a scalar control volume, and the three momentum equations are integrated over respective (staggered) velocity component control volumes. The derivatives in the diffusion terms are discretized using second-order-accurate central difference approximations, whereas the velocities in the convection terms are interpolated to the faces of the control volumes by means of the quadratic upstream weighted scheme proposed by Leonard [14]. This scheme is formally third-order accurate and has good stability properties.

The numerical solution of the resulting time-dependent system of ordinary differential equations is obtained using a second-order accurate, explicit, Runge–Kutta predictor-corrector method (RK2). The numerical procedure is globally second-order accurate, but does not require the storage of both velocity and pressure fields at two previous time levels. The strategy

followed to calculate the pressure field is based on an idea formulated by Chorin [15], wherein the velocity field at each new time step is decomposed into two contributions, one involving and the other not involving the pressure field. The pressureless contribution is calculated directly using the RK2 algorithm. The pressure contribution is calculated by solving the discrete Poisson equation for the pressure that results from the imposition of the divergence-free condition for the velocity field (mass conservation equation) at the end of each half-time step. This second step is achieved through the use of a conjugate gradient procedure.

2.3. Additional code testing

The extensive testing of the numerical algorithm has been discussed in Humphrey *et al.* [6]. However, because it is important to establish confidence in the accuracy of the procedure as applied to the present problem, we mention two specific tests documented in Reference [13]. The first test consists of the buoyancy-assisted flow past a backward-facing step in a vertical channel. It is implemented according to the benchmark specifications of Blackwell and Armaly [16]. The reader is referred to that reference for a description of the problem and the results obtained by various authors. In particular, the velocity and temperature results obtained by Iglesias *et al.* [17] are in excellent agreement with the reference standard.

The second test corresponds to one of the experimental cases investigated by Szeri *et al.* [18]. It provides axial profiles of the circumferential and radial velocity components measured with an LDV at various radial locations for the flow of water in the space between two rotating disks. With reference to Figure 1, the dimensions of the experimental apparatus are: $R_2 = 25.4$ cm, $R_1 = 1.69$ cm, and $H = 1.26$ cm. For the test discussed here, the bottom disk and the enclosure wall rotate at 2.72 rpm while the top disk and central hub are stationary. The Reynolds number of the flow based on the radius and angular velocity of the rotating disk is $Re = 21\,260$. After preliminary grid testing, an 80×34 $(r{-}z)$ grid was used in the final calculation, with an axisymmetric condition imposed in the circumferential direction. Figure 2 compares measured and calculated velocity component profiles. The agreement between the two sets of velocity data is excellent, with somewhat less satisfactory agreement obtained for the radial velocity component. This relatively small discrepancy is attributed to an unavoidable uncertainty associated with the numerical implementation of the experimental exit flow boundary condition [13].

2.4. Calculation grids

For the configurations of interest here, the grid nodes are distributed non-uniformly throughout the calculation domain in order to resolve the strongly sheared regions of the flow. These regions are: the Ekman layers along the respective disk surfaces, the shear layer along the fixed cylindrical enclosure wall, and the detached shear layer lying between the region of flow in solid body rotation and the fully three-dimensional potential core. Estimates of the location and size of these regions provided in References [4,6,7] were used to construct the present grids. This approach permits an effective distribution of nodes while avoiding unnecessary refinement where velocity gradients are weak, e.g. in the solid body rotation region. Because the thickness of the shear layers varies with disk angular velocity, and because all the grids are generated to accommodate at least five nodes in the various shear layers, the grids differ among the cases calculated. However, the non-uniform distribution of nodes is similar in all cases [13].

The axisymmetric calculations were performed on a 70×40 $(r{-}z)$ grid when $\Gamma = 0.186$ and a 70×50 $(r{-}z)$ grid when $\Gamma = 0.279$. A grid dependence study was performed for two of the

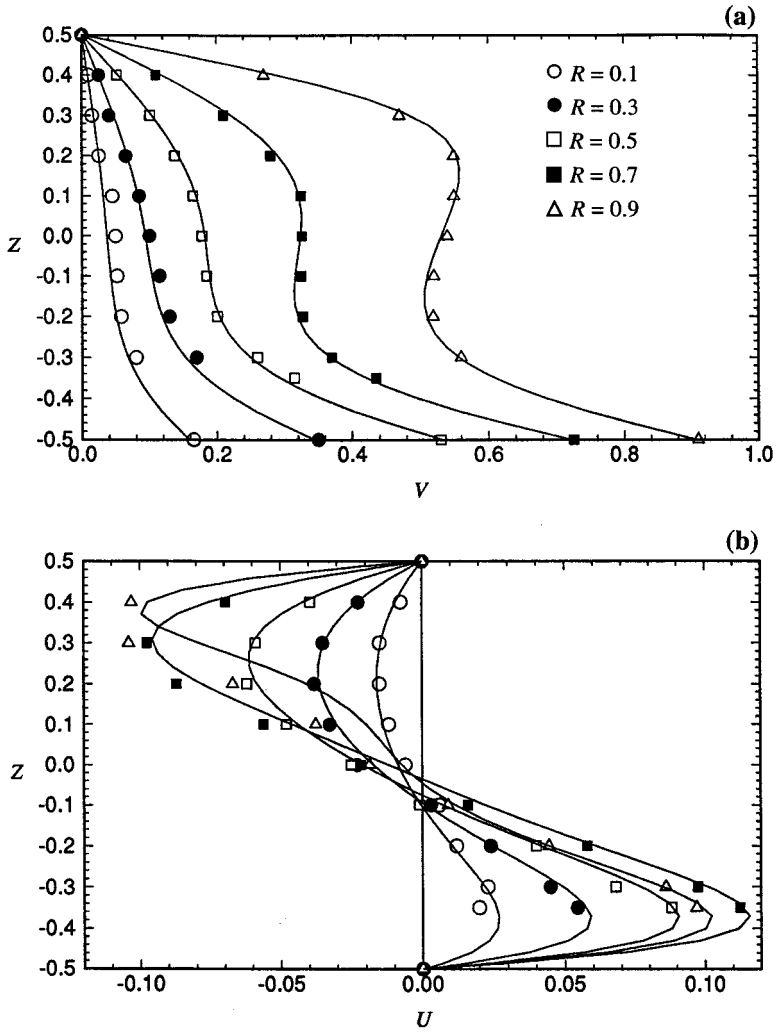

Figure 2. Axial profiles at five radial positions of non-dimensional (a) circumferential and (b) radial velocity components. The top disk (at $Z = 0.5$) and the central hub (at $R = 0$) are stationary, whereas the bottom disk (at $Z = -0.5$) and the enclosure wall (at $R = 1$) rotate with $Re = 21\,259$. Solid lines correspond to numerical results and symbols to the experimental data of Szeri *et al.* [18].

axisymmetric cases considered. For the first case, with $\Gamma = 0.186$ and $Re = 23\,150$, an oscillatory periodic flow was calculated on the 70×40 grid and on an 80×50 $(r-z)$ grid. The frequency and magnitude of the oscillations were found to differ by less than 5% and 2%, respectively, and the average torque coefficient showed a discrepancy of less than 0.1% between these two grids. For the second case with $\Gamma = 0.279$ and $Re = 11\,570$, a steady flow was calculated on the 70×50 $(r-z)$ grid and on an 80×60 $(r-z)$ grid. The comparison between velocity profiles for these two grids was excellent, and the same torque coefficient was obtained.

Due to limited computer time and storage, the same number of nodes in the $r-z$ plane could not be used for the three-dimensional calculations. Consequently, coarser cross-stream grids were set, consisting of 56×26 $(r-z)$ nodes when $\Gamma = 0.186$ and 56×36 $(r-z)$ nodes when

$\Gamma = 0.279$. Axisymmetric calculations performed on these grids yielded results estimated to be within 5–7% of grid independence and in excellent qualitative agreement with the more refined grids above. The θ grid consisted of 48 nodes uniformly distributed in the circumferential direction. Because of the limitations referred to, it was not possible to perform meaningful grid refinement tests for the θ direction. However, calculations by Herrero (personal communication, 1994), obtained with the CUTEFLOWS program for the flow configuration of Figure 1, with $H = 9.53$ mm, $R_1 = 56.4$ mm, $R_2 = 105$ mm, $a = 0$ and $Re = 20\,000$, show that, whereas the details of the calculated flow field depend on the degree of θ refinement, all three-dimensional features of the unsteady flow are correctly captured using 48 nodes in the θ direction. The present three-dimensional grid, for $\Gamma = 0.186$ is 1.5 times more refined in the θ direction and 1.72 times more refined globally than the grid used in [6].

The distribution of grid nodes sets an upper limit on the allowable time step, Δt, used by the present explicit calculation procedure. A typical time step, $\Delta t = 10^{-4}$ s, was used when it was shown that smaller values had a negligible influence on the calculated results. The numerical evaluation of one time step on the grids used typically required between 5.5 and 7.5 s.

3. RESULTS AND DISCUSSION

The flow configuration of interest is investigated with respect to the aspect ratio and the Reynolds number; the former by varying the interdisk spacing, H, and the latter by varying the rotation rate, Ω, since the radial dimensions of the disks and the fluid properties are kept constant. The strategy used in the investigation is as follows. Fixing the aspect ratio, the Reynolds number is varied over a prescribed range. As the Reynolds number varies, variations may occur in the qualitative structure of the solutions for certain values of this parameter. These are called bifurcations, and they involve changes in the number of solutions, as well as in their stability.

The configuration dimensions are given in Figure 1 and correspond to values of $\Gamma = 0.186$ and 0.279, respectively. The rotation rates investigated are: 50, 100, 150, 200 and 300 rpm, corresponding to $Re = 3858$, 7715, 11 570, 15 430 and 23 150. The radial clearance between the rim of a disk and the cylindrical enclosure wall is taken as $a = 0$ in most of the calculations. Axisymmetric calculations are also performed for the configuration of Figure 1, with $a = 2.7$ mm, $b = 1.91$ mm and $H = 9.53$ mm ($\Gamma = 0.186$) for rotation rates of 100 and 200 rpm ($Re = 7335$ and 14 670). We now present and discuss the results of the axisymmetric and three-dimensional calculations for the various cases considered. The results show major differences between the characteristics of the flow for the two aspect ratios.

3.1. Aspect ratio $\Gamma = 0.186$

3.1.1. Two-dimensional (axisymmetric) flow. For $Re \leq 15\,430$, the axisymmetric flow reaches a steady symmetric state with respect to the interdisk mid-plane, irrespective of the initial calculation condition or the imposition of perturbations. The flow perturbation consists of a 5% increase in the rotational speed of the upper disk (to rotate at 1.05 Ω) and a 5% decrease in the rotation of the lower disk (to rotate at 0.95 Ω) for a period of time usually corresponding to five revolutions of the disks. This perturbation is consistently axisymmetric, but breaks the flow symmetry about the mid-plane in the axial direction. The perturbation decays rapidly and the calculated flow field attains the symmetric steady state presented in Figure 3. (Note that the velocity vectors in the figure are plotted only for alternate grid nodes

in both co-ordinate directions, and a reference vector of non-dimensional magnitude 0.1 is shown.) In the contour plots, solid lines represent positive values of the variable and dashed lines represent negative values. In the streamline plot, a clockwise flow recirculation is represented by negative values of the streamfunction, defined in Equation (9).

In contrast, the axisymmetric flow at $Re = 23\,150$ oscillates periodically about the interdisk mid-plane. Figure 4 shows the flow field at an instant in time. The oscillation develops without the imposition of a perturbation. Figure 5 shows the time variation of the non-dimensional axial velocity component at a monitoring point located on the interdisk mid-plane. Due to the periodic change in sign of the axial velocity component with respect to the mid-plane, its frequency is half that of the other two velocity components and pressure which do not change sign. Power spectra of these time series (calculated using data for $\Omega t \geq 150$ only) reveal a pair of dominant frequencies in this flow, namely $2\pi f/\Omega = 0.83$ for U and V, and 0.415 for W. Harmonics arise in the spectra for U and V.

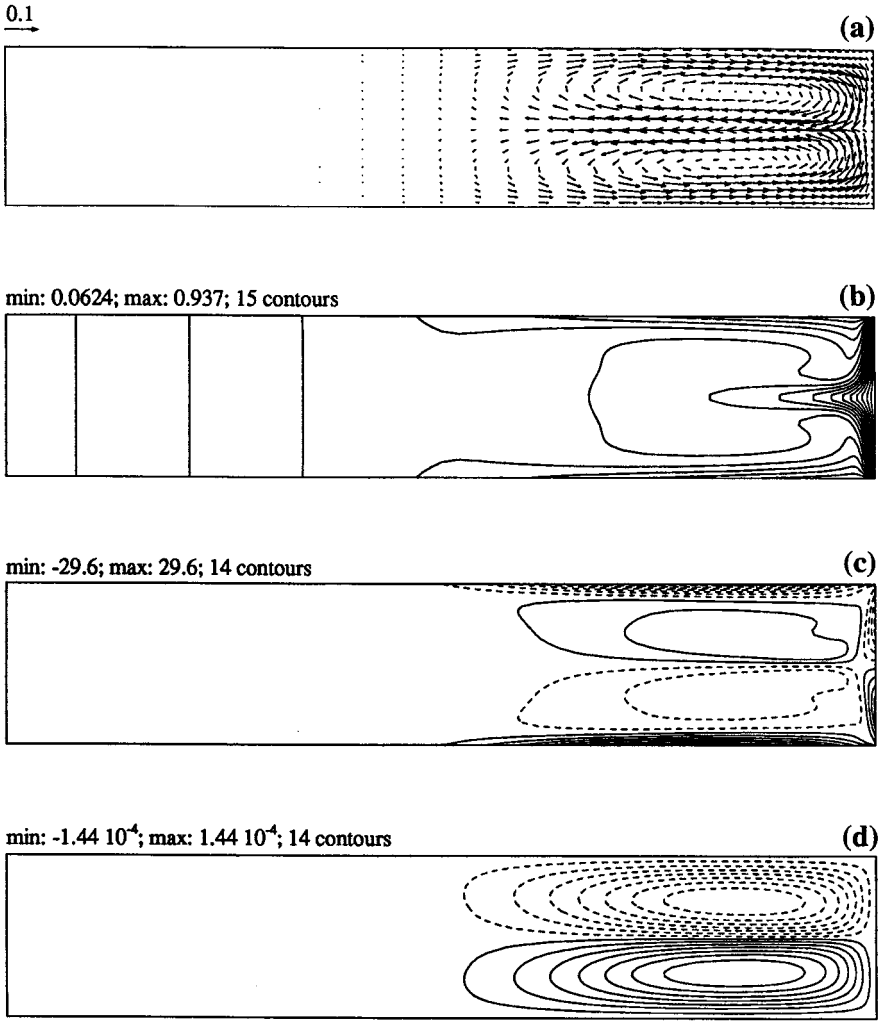

Figure 3. Plots of the axisymmetric steady cross-stream (r–z) plane flow for $\Gamma = 0.186$ and $Re = 15\,430$: (a) cross-stream velocity vectors; (b) circumferential velocity contours; (c) circumferential vorticity contours; and (d) cross-stream flow streamlines.

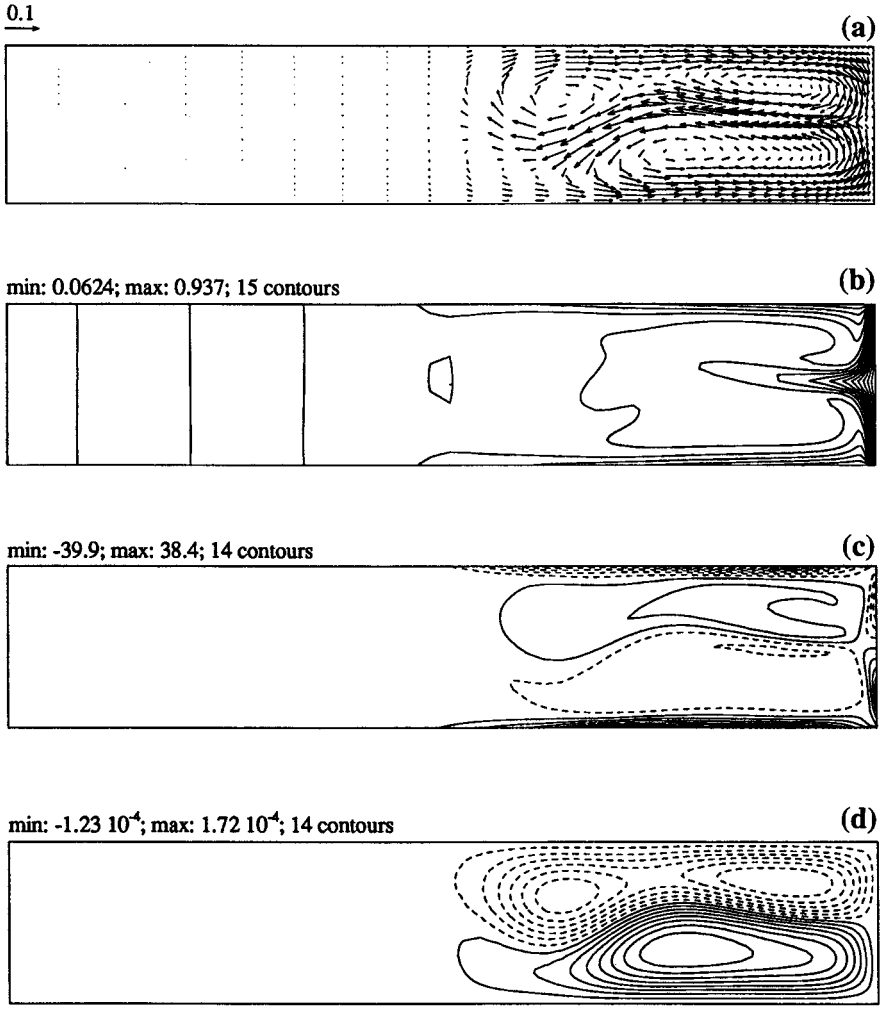

Figure 4. Plots of the axisymmetric unsteady cross-stream (r–z plane) flow at a particular instant in time for $\Gamma = 0.186$ and $Re = 23\,150$. The flow is oscillatory periodic everywhere about the interdisk mid-plane: (a) cross-stream velocity vectors; (b) circumferential velocity contours; (c) circumferential vorticity contours; and (d) cross-stream flow streamlines.

3.1.2. Effects of disk-enclosure gap and disk thickness. Axisymmetric calculations were also performed for the configuration shown in Figure 1, with $R_1 = 56.4$ mm, $R_2 = 105$ mm, $H = 9.53$ mm, $a = 2.7$ mm and $b = 1.91$ mm, in order to assess the effects of the disk rim–enclosure wall gap on the flow. These dimensions yield the same aspect ratio, $\Gamma = 0.186$, as the previous configuration with $a = 0$ and $R_2 = 107.7$ mm. This case was calculated for $Re = 7335$ and 14 670. Two boundary conditions (described above) were explored for the gap: symmetry and periodicity. For $Re = 7335$, the same steady state solution was obtained irrespective of the gap boundary condition. For $Re = 14\,670$, the flows predicted differed for the two boundary conditions, but both were oscillatory periodic, in contrast to the steady symmetric flow calculated for $Re = 15\,430$ with $a = 0$ and $R_2 = 107.7$ mm.

Instantaneous circumferential vorticity contours for the axisymmetric oscillatory flow calculated at $Re = 14\,670$ using the periodic boundary condition in the gap are shown in Figure 6 at four instants in time. A significant difference between the flows calculated using the two respective gap boundary conditions pertains to the radial extension of the solid body rotation region. The penetration of this region radially outward is larger for the flow with the symmetry boundary condition in the gap than for the flow with the periodic boundary condition imposed. The solution obtained using the periodic boundary condition yields a location of the detached shear layer (see Figure 1) that closely matches the location predicted by the experimental correlation of Humphrey and Gor [7].

Another striking difference between the flows calculated using the two different gap boundary conditions arises with respect to the magnitude of the axial oscillation of the stagnation point marking the location on the enclosure wall where the redirected Ekman layers collide. The stagnation point oscillates with a higher amplitude when the symmetry condition is imposed in the gap. For the periodic boundary condition, the stagnation point oscillates closer to the mid-plane and the meandering of the radial jet emerging from the enclosure wall region is smaller. This second condition is in closer accord with experimental observations and with the axisymmetric oscillatory flow calculated where $a = 0$ and $Re = 23\,150$.

For both sets of boundary conditions, the resulting flows display small recirculation regions in the gap. The recirculation regions oscillate along the enclosure wall and, in the case of the flow calculated using the periodic boundary condition, detach from the disk rim. These motions induce additional frequencies in the power spectra of the monitoring variables. For the periodic boundary condition their frequency is considerably higher than for the symmetry boundary condition, and there are fewer harmonics in the power spectra. With the symmetry boundary condition imposed in the gap, these oscillations are not exactly symmetric about the interdisk mid-plane. This is in contrast with the periodic boundary condition, for which symmetric oscillations are obtained [13].

3.1.3. Three-dimensional (non-axisymmetric) flow. Three-dimensional calculations were performed for a configuration very similar to that investigated numerically by Humphrey *et al.* [6], in which the effects of the disk rim–enclosure wall gap were considered but the thickness of the disks was neglected. The configuration is defined by setting $R_1 = 56.4$ mm, $R_2 = 105$ mm, $a = 2.7$ mm, $H = 9.53$ mm and $b = 0$ in Figure 1, and fixing a symmetry boundary condition

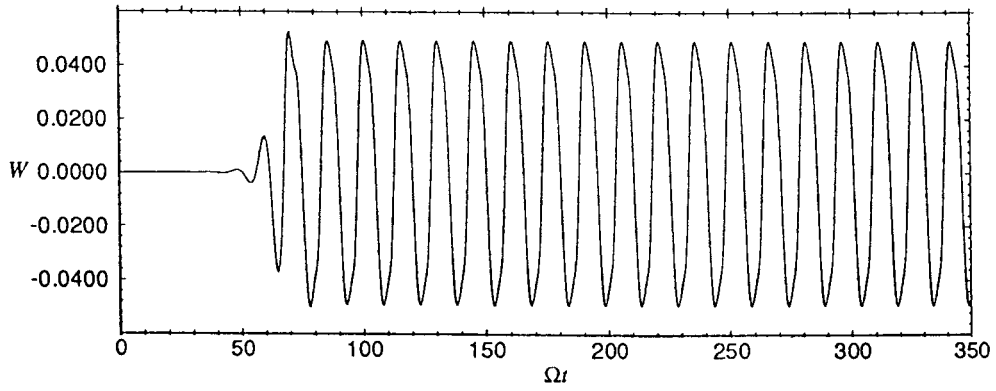

Figure 5. Time variation of the axial velocity component at a monitoring point with co-ordinates $R = 0.573$ and $Z = 0$ for the axisymmetric unsteady flow, with $\Gamma = 0.186$ and $Re = 23\,150$.

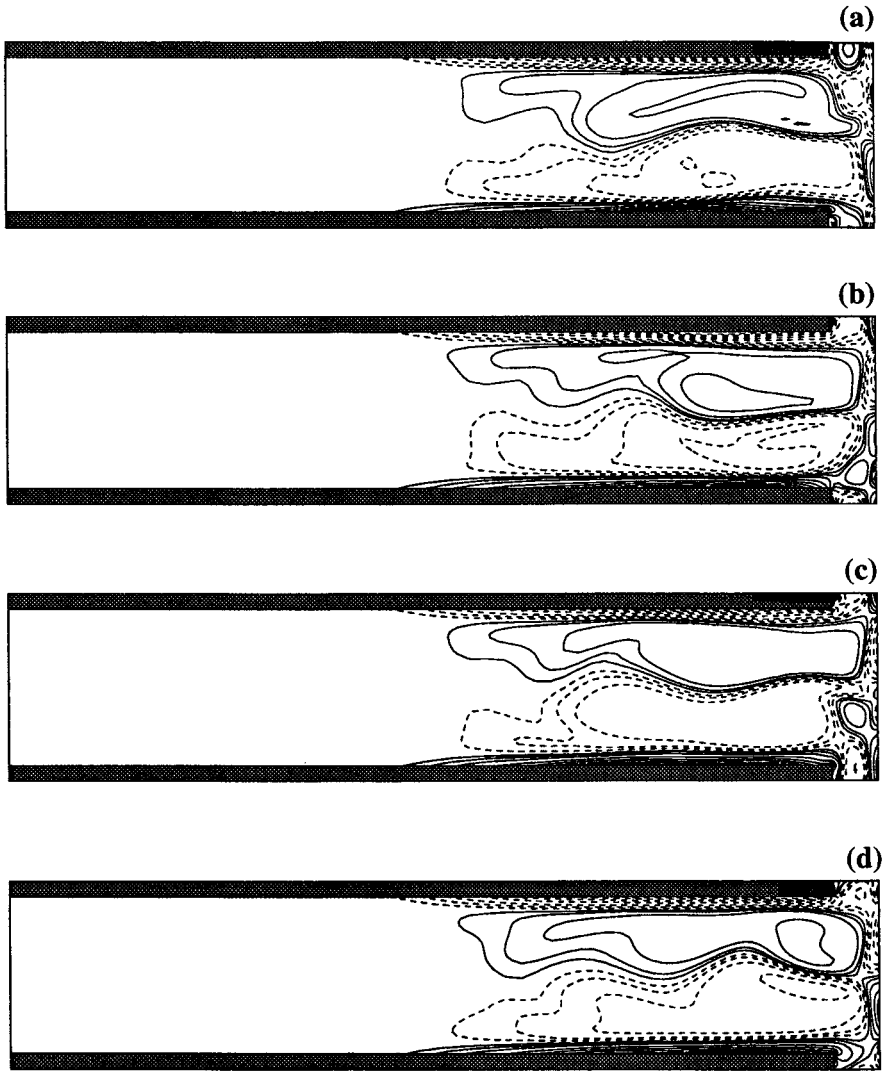

Figure 6. Contours of the circumferential vorticity component at four instants in time for the axisymmetric oscillatory periodic flow corresponding to the configuration of Figure 1 with the periodic boundary condition imposed in each gap ($R_1 = 56.4$ mm, $R_2 = 105$ mm, $a = 2.7$ mm, $b = 1.91$ mm), $\Gamma = 0.186$ ($H = 9.53$ mm), and $Re = 14\,670$: (a) $\Omega t = 0$ (arbitrarily chosen); (b) $\Omega t = 1.68$; (c) $\Omega t = 3.14$; (d) $\Omega t = 5.86$. The contour levels correspond to $\omega_\theta = 35$, 30, 25, 20, 15, 10, 5, 2.5 and 1.

in the gap. The configuration has been calculated in this study for the same aspect ratio and rotational speed (300 rpm, in this case corresponding to $Re = 23\,150$), but setting $R_2 = 107.7$ mm and $a = 0$ to provide a reference for comparison with the results obtained for the flow configuration in which $\Gamma = 0.279$, presented below. The present calculation is performed on a grid 1.5-fold more refined in the circumferential direction than the $31 \times 41 \times 32$ (r–z–θ) grid used by Humphrey *et al.*, who predict four foci of intensified axial vorticity in a prematurely terminated calculation with $Re = 22\,200$ and six foci in a converged calculation with $Re = 44\,400$.

Results of the present converged calculation in the form of instantaneous contours of the axial vorticity component, ω_z, on the interdisk mid-plane are shown in Figure 7. (By converged we mean that the present flow acquired a steady periodic state with primary oscillation frequencies corresponding to $2\pi f/\Omega = 3.4$ for the radial and axial velocity components and $2\pi f/\Omega = 1.7$ for the circumferential). The contour levels plotted were specifically selected to display the circumferentially periodic foci of positive axial vorticity described by Humphrey *et al.* [6]. Large negative values of ω_z (the dashed lines in the figure) arise due to the action of viscous shear along the fixed enclosure wall and are confined to the wall shear layer. In the region of solid body rotation, ω_z assumes small positive values up to the location of the detached shear layer, where it drops abruptly to negative values. In the potential flow region the values of ω_z range from -0.5 to 0.5, approximately, and the positive axial vorticity component is concentrated in eight circumferentially periodic foci. As described by Humphrey *et al.*, the foci are due to the radial/circumferential variations of the circumferential velocity component. Experimentally, their number is believed to be ten in the range $20\,000 < Re < 40\,000$. Apart from the number of foci and other details resolved on the present finer grid, the characteristics of this flow case agree with the findings of Humphrey *et al.* [6].

3.2. Aspect ratio $\Gamma = 0.279$

3.2.1. Two-dimensional (axisymmetric) flow. The cases in this section correspond to the configuration of Figure 1, with $R_1 = 56.4$ mm, $R_2 = 107.7$ mm, $a = 0$ and $H = 14.3$ mm. For all values of the Reynolds number explored, the resulting flow reaches a steady state. At the lowest Reynolds number, $Re = 3858$, the flow is symmetric, as for the case where $\Gamma = 0.186$, when $Re \leq 15\,430$. A calculation for $Re = 5788$ also reveals a steady symmetric flow of similar

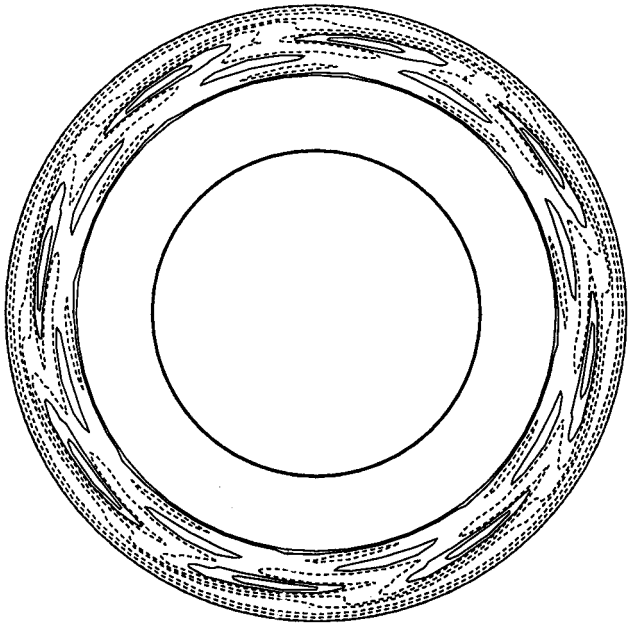

Figure 7. Instantaneous contours of the axial vorticity component on the interdisk mid-plane for the three-dimensional unsteady flow with $\Gamma = 0.186$ and $Re = 23\,150$. The contour levels correspond to $\omega_z = -20, -5, -1, \pm 0.5$ and ± 0.1. In this and subsequent plan views, the inner circle in the figure represents the hub periphery. The hub and disks rotate in the counterclockwise direction.

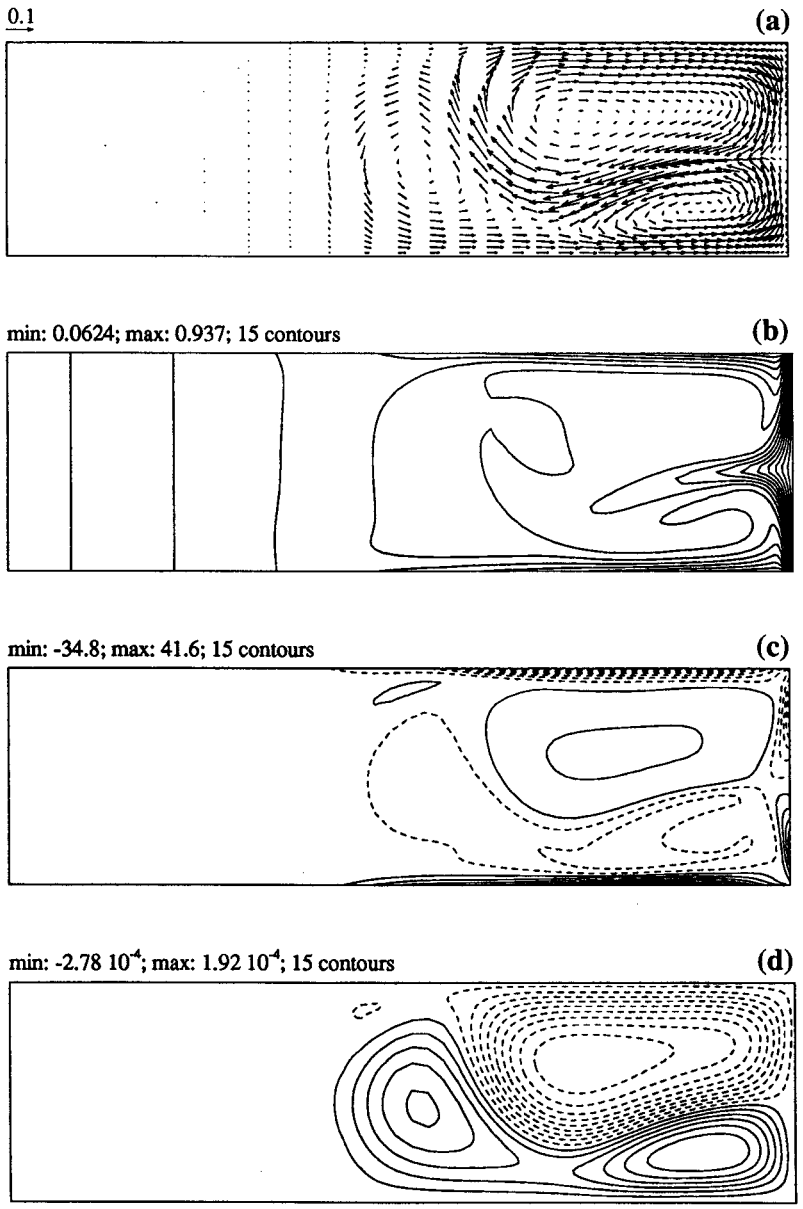

Figure 8. Plots of the axisymmetric steady cross-stream (r–z plane) flow for $\Gamma = 0.279$ and $Re = 15\,430$: (a) cross-stream velocity vectors, (b) circumferential velocity contours, (c) circumferential vorticity contours, and (d) cross-stream flow streamlines.

characteristics. However, between $Re = 7715$ and $Re = 23\,150$, the flow loses its symmetry about the interdisk mid-plane while approaching a steady state. Figure 8 shows the final steady cross-stream (r–z plane) motion for $Re = 15\,430$. In the figure, the velocity vectors are plotted only for alternate grid nodes in each direction. Figure 9 shows the time variation of the axial velocity component at a monitoring point located on the interdisk mid-plane. This plot, corresponding to $Re = 7715$, shows a smooth evolution of the flow towards the asymmetric steady state ultimately acquired.

The results in Figure 8 correspond to one of two solutions found for the case where $\Gamma = 0.279$ and $Re = 15\,430$. The prediction of pairs of flow fields that are mirror images of each other was typical. Of the two solutions, the one obtained seemed to be an arbitrary outcome, even when the initial condition for the calculation was a deliberately imposed, slightly asymmetric flow field. (The axisymmetric disk-driven perturbation described at the beginning of Section 3.1 was applied to every developed flow field. When the perturbation was discontinued, the flow evolved, with equal probability, either to its original solution or to the mirror image of that solution.) Although the calculated flow in this study has not been experimentally observed in rotating disk systems, similar asymmetric solutions have been found to be physically realizable in Taylor–Couette flow experiments [19]. The imposed axisymmetry constraint may play an important role in determining the flow structure. The three-dimensional calculations presented below show that when this constraint is relaxed, the calculated flow oscillates about the interdisk mid-plane, as observed in previous studies [7]. Calculations not shown here, carried out in a flow configuration with $\Gamma = 0.279$ but including the disk rim–enclosure wall gap and the disk thickness ($R_1 = 56.4$ mm, $R_2 = 105$ mm, $a = 2.7$ mm, $H = 14.3$ mm and $b = 1.91$ mm), lead to the conclusion that these geometrical features are probably not responsible for the particular behavior found [13].

3.2.2. Three-dimensional (non-axisymmetric) flow. With the aim of finding similarities between flows with different aspect ratios, we consider the alternative definition of the Reynolds number, Re_H ($= \Omega R_2 H/v$), which should be more representative of the cross-stream motion characteristics. The value of Re_H where $\Gamma = 0.279$ and $Re = 15\,430$ is $Re_H = 2049$. This value of Re_H is virtually identical to that of the three-dimensional flow, with $\Gamma = 0.186$ and $Re = 23\,150$ ($Re_H = 2048$) presented in the previous section. Therefore, a calculation of the flow with $\Gamma = 0.279$ and $Re = 15\,430$ is expected to yield a three-dimensional solution.

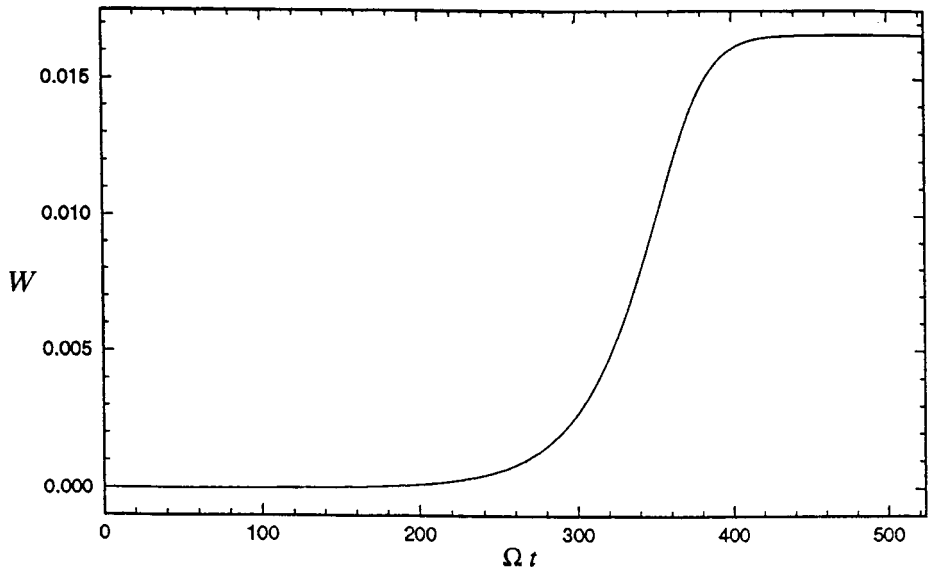

Figure 9. Time variation of the axial velocity component at a monitoring point with co-ordinates $R = 0.575$ and $Z = 0$ for a flow with $\Gamma = 0.279$ and $Re = 7715$. Below $\Omega t \simeq 200$, the flow is steady and symmetric with respect to the interdisk mid-plane. Above $\Omega t \simeq 200$, it is steady and axisymmetric with respect to the mid-plane.

A preliminary calculation of this flow was performed using the previously calculated axisymmetric velocity field shown in Figure 8 as the initial condition. With no perturbation applied to this initial flow field, the result after 0.1 s (one-third of a disk revolution) simply confirmed the solution provided initially. Thus, the axisymmetric solution was shown to satisfy the conservation equations even when the axisymmetric condition was relaxed. To break the axisymmetry of the flow field, a non-axisymmetric perturbation ($w|_{\text{disk}}$) was applied in the form of a simulated wobble of the disks. The perturbation was imposed for 0.1 s and was circumferentially sinusoidal, with an amplitude 5% of the local disk speed: $w|_{disk} = 0.05\,\Omega\, r \sin\theta$. This axial velocity was applied in phase to both disks in such a way that global continuity was preserved. The result was an irregular (non-periodic) oscillatory flow field. The calculation was repeated with a quiescent fluid as an initial condition, and a similar irregular oscillatory flow was obtained. This ensured that the initial condition was not a factor in determining the fully developed flow.

In contrast to the lack of symmetry about the interdisk mid-plane, which is exhibited by the axisymmetric solution of this flow configuration, the fully three-dimensional solution reveals oscillations which are on average symmetric about the mid-plane, even though they result in irregular variations of the velocity components. Cross-stream vector velocity fields plotted in Figure 10 for different r–z planes 22.5° apart show that the jet of fluid directed along the radial direction from the enclosure wall into the potential core oscillates about the mid-plane. The resulting extremes of this flow field are very similar to those predicted as steady states in the axisymmetric calculations. The oscillations are stronger in this case ($\Gamma = 0.279$ and $Re = 15\,430$) than with the smaller aspect ratio ($\Gamma = 0.186$ and $Re = 23\,150$), even though these two cases possess the same Re_H. Unsteadiness appears at a lower value of Re_H, and the magnitude of the oscillations is larger for the flow configuration with $\Gamma = 0.279$. Humphrey and Gor [7] have shown that for the same Reynolds number, the flow with larger Γ is more prone to instability. These results suggest that Re_H is not a sufficient parameter to guarantee complete flow similarity.

Figure 11 shows the distribution of the axial vorticity component on the interdisk mid-plane. This is irregular, and a single characteristic wave number cannot be determined. However, even though the circumferential extensions of the vortical foci vary, an even integer number (six) of well-defined foci is clearly identified. Two of the foci are elongated in the circumferential direction, as if each were going to split into sub-foci pairs. Figure 12(b) shows the corresponding time variation of the axial velocity component for this irregular flow at a monitoring point on the interdisk mid-plane.

3.2.3. Variation with Reynolds number (disk rotational speed). The effect on the developed flow field due to changing the Reynolds number (by altering Ω) was considered by calculating the cases with $Re = 7715$ (100 rpm) and $Re = 23\,150$ (300 rpm). Isocontours of the axial vorticity component on the interdisk mid-plane are plotted in Figure 13 for the higher Re case. Contrasting these results with those for the three-dimensional flow where $Re = 23\,150$ and $\Gamma = 0.186$ (Figure 7), illustrates the increased disorderliness of the foci structure and location with increasing Γ. For $\Gamma = 0.279$ the number of foci appears to vary with time, ranging between six and eight, and they are strongly distorted in both the circumferential and radial directions. The six foci observed in the flow with $Re = 7715$ and $\Gamma = 0.279$ were much more ordered [13]. Time variations of the axial velocity component at proximal monitoring points on the interdisk mid-plane (Figure 12) show that past the initial transient, the flow evolves from time periodic at $Re = 7715$ to increasingly irregular for $Re \geq 15\,430$.

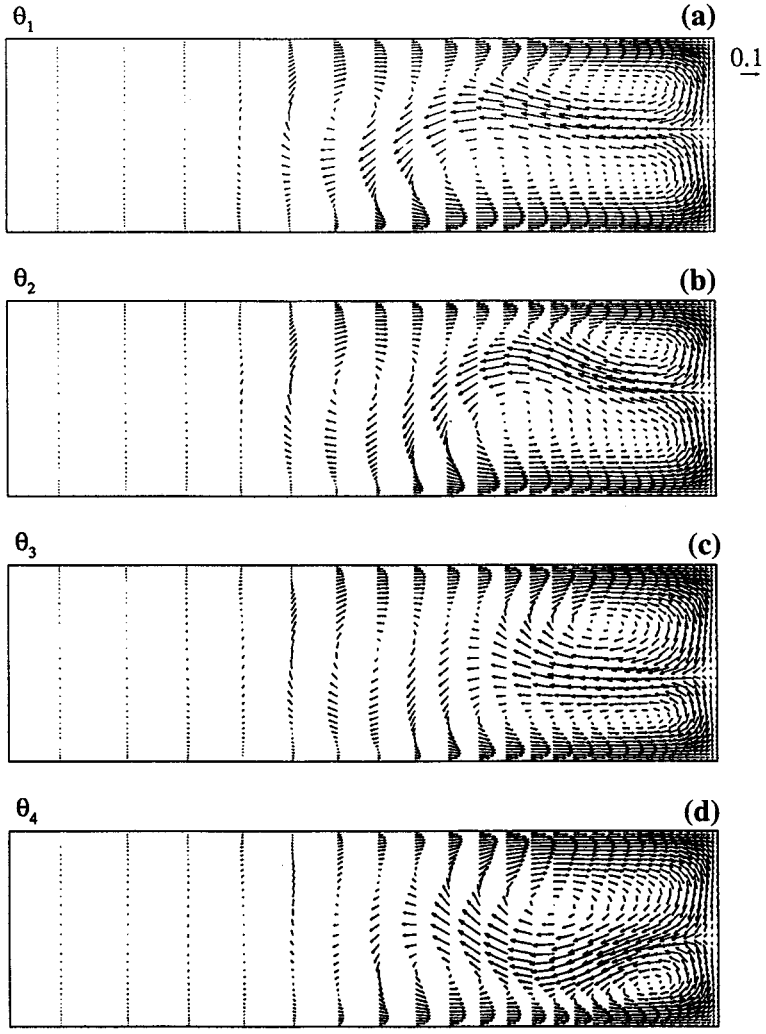

Figure 10. Velocity vector fields at cross-stream (r–z) planes 22.5° apart for the three-dimensional unsteady flow with $\Gamma = 0.279$ and $Re = 15\,430$. For clarity, vectors are plotted on alternate grid nodes in the radial direction.

4. CONCLUSIONS

Experimental investigations show that in a critical range of Reynolds number the flow between a pair of disks co-rotating in a fixed cylindrical enclosure evolves from steady axisymmetric to unsteady three-dimensional. For a geometry with $\Gamma = 0.186$ the range is $4580 < Re < 4880$ and for one with $\Gamma = 0.279$ it is $3700 < Re < 4440$. The unsteady three-dimensional flow is characterized by the presence of foci of intensified axial components of vorticity distributed periodically in the circumferential co-ordinate direction. The number of foci appears always to be even and decreases in a stepwise manner with increasing Re. For a geometry with $\Gamma = 0.186$ the number of foci is believed to be ten for $20\,000 < Re < 40\,000$, approximately. The foci rotate at a speed ranging between 0.5 and 0.8 of the angular velocity of the disks, depending on the details of the flow geometry. All the above values are for a configuration with a finite

disk rim–enclosure wall spacing of $a/H = 0.28$ or, equivalently, $a/R_2 = 0.026$. However, the evidence is that the number and distribution of the foci do not depend critically on the presence of this gap for such small values.

Numerical calculations have been performed for the above two flow configurations, with $a/H = 0$. The calculations were first performed imposing the axisymmetry condition on the conservation equations, and then with this condition relaxed. The following findings apply:

(1) For the case with $\Gamma = 0.186$ and with axisymmetry imposed, the calculated flow is steady and symmetric about the interdisk mid-plane when $Re \leq 15\,430$. Attempts to perturb the symmetry of the flow below this value of Re failed. When $Re = 23\,150$, the flow oscillates periodically about the interdisk mid-plane without needing to be perturbed. Calculations with $Re = 23\,150$ and with the axisymmetry requirement relaxed yield an unsteady three-dimensional flow with eight foci of intensified axial vorticity evenly distributed in the circumferential co-ordinate direction. Earlier three-dimensional calculations for this condition on a coarser grid [6], yielded four foci when $Re = 22\,000$ and six when $Re = 44\,400$. In contrast, the experimental evidence is for ten foci in the range $20\,000 < \mathrm{Re} < 40\,000$. The closer correspondence with reality in the present work is attributed to the finer grids used.

(2) For the case with $\Gamma = 0.279$ and with axisymmetry imposed, steady flow fields are predicted for all values of the Reynolds number. In the range $7715 \leq Re \leq 23\,150$, however, the flow evolves from a symmetrical to an asymmetrical state with respect to the interdisk mid-plane. Numerical experiments for the case with $Re = 15\,430$ reveal that mirror-image solutions (with respect to the mid-plane) can be arbitrarily obtained irrespective of the starting flow conditions or the imposition of perturbations. Calculations with $Re = 15\,430$ and with the axisymmetry requirement relaxed yield an unsteady three-dimensional flow with six foci of intensified axial vorticity irregularly distributed in the circumferential co-ordinate direction.

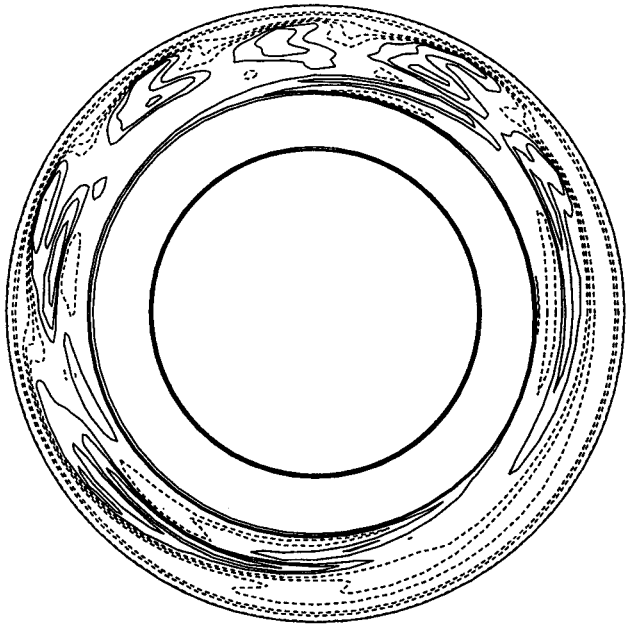

Figure 11. Instantaneous contours of the axial vorticity component on the interdisk mid-plane for the three-dimensional unsteady flow with: $\Gamma = 0.279$ and $Re = 15\,430$. The contour levels correspond to $\omega_z = -10,\ -5,\ \pm 1,\ \pm 0.5$ and ± 0.2.

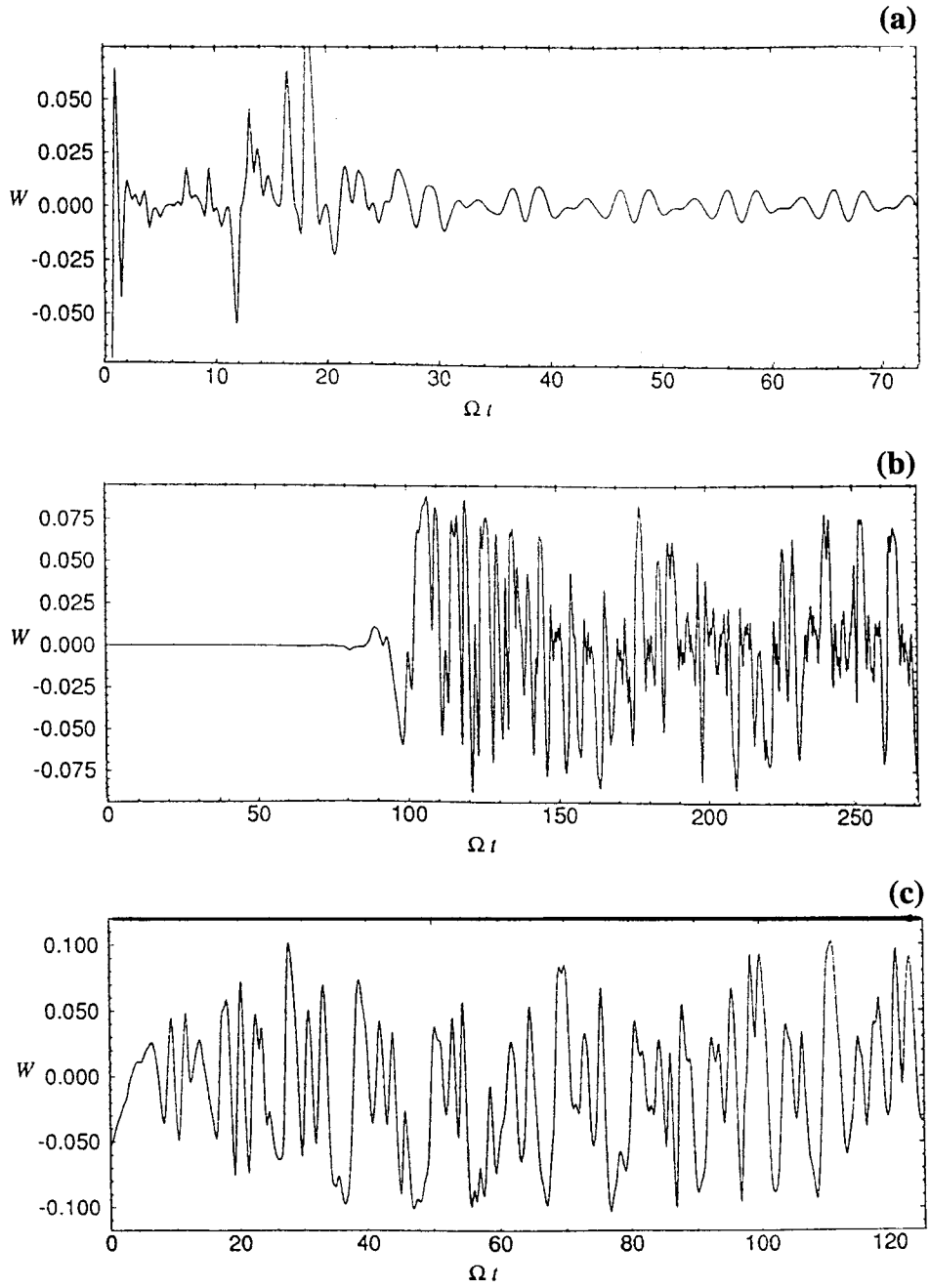

Figure 12. Time variation of the axial velocity component at a monitoring point located at $\theta = 0$, $Z = 0$ and proximal R co-ordinates for $\Gamma = 0.279$: (a) $Re = 7715$ and $R = 0.523$; (b) $Re = 15\,430$ and $R = 0.574$; (c) $Re = 23\,150$ and $R = 0.597$.

The structure of the foci is also irregular and appears to vary with time. The onset of flow unsteadiness for this case was induced by a numerically imposed wobble of the disks. Further increasing the Reynolds number to 23 150 yields an even more disorderly time-dependent flow with between six and eight foci of vorticity. In contrast, decreasing the Reynolds number to 7715 restores an oscillatory periodic flow condition with six (more evenly spaced) foci of axial vorticity. Unfortunately, for the case with $\Gamma = 0.279$ there are no measurements of the number of foci as a function of the Reynolds number. Nevertheless, the experimental evidence is that, for Re fixed, the number of foci decreases with increasing Γ. This condition seems to be preserved in the present calculations.

The effect on the flow field due to the presence of a finite disk rim–enclosure wall gap was investigated for the configuration with $\Gamma = 0.186$ and the axisymmetry condition imposed. The size of the gap was set to $a/H = 0.28$, corresponding to the geometrical condition of earlier experimental and numerical work. Two gap boundary conditions, flow symmetry and periodicity, were explored. For $Re = 7335$ essentially identical steady flow fields are predicted for the two boundary conditions. For $Re = 14\,670$ the details of the flow fields, especially near the disk rim, depend on the boundary condition specified, but both cases yield oscillatory periodic flow. In contrast, the flow in the configuration with $a = 0$ and $Re = 15\,430$ is steady and symmetric, indicating that the presence of a gap lowers the threshold for transition to unsteady motion. Both sets of gap boundary conditions yield small regions of recirculating cross-stream flow in and around the gap. These are observed to oscillate axially along the enclosure wall and, in the case with the periodic boundary condition, detach from the disk rim. Of the two conditions, the periodic boundary, yields flow characteristics in better accord with experimental observations and numerical calcula-

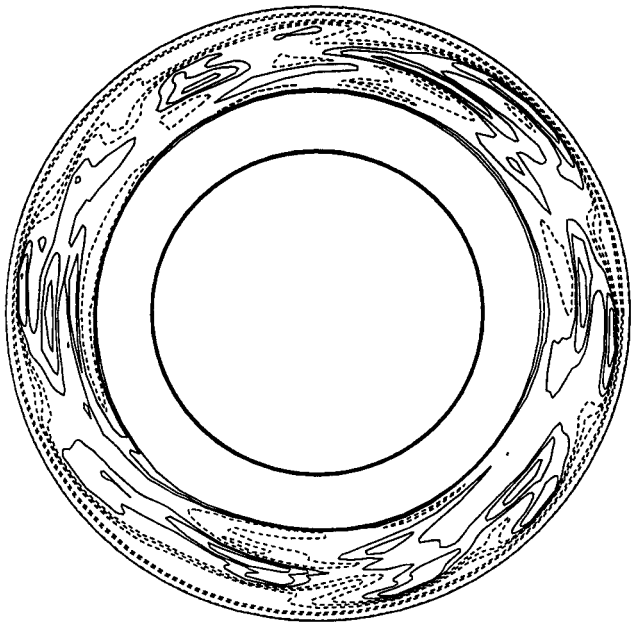

Figure 13. Instantaneous contours of the axial vorticity component on the interdisk mid-plane for the three-dimensional unsteady flow with $\Gamma = 0.279$ and $Re = 23\,150$. The contour levels correspond to $\omega_\theta = -10,\ -5,\ \pm 1,\ \pm 0.5$ and ± 0.02.

tions with $a = 0$. However, it is important to note that whereas the presence of a gap may help trigger the transition from steady symmetric flow to unsteady three-dimensional flow at lower values of *Re* than those calculated, the gap seems to have little if any effect on the number of vortical foci generated because of its relatively small size.

In this study, special care has been taken to generate numerical results which, while not free of false diffusion, are accurate enough to place all of the observations presented on a firm basis.

ACKNOWLEDGMENTS

The first author acknowledges Fulbright-La Caixa, and CIRIT of the Generalitat de Catalunya, who awarded her with fellowships during her stay at the University of California at Berkeley. Partial support for the project was provided by the Computer Mechanics Laboratory (CML) of the University of California at Berkeley, where the study was initiated. Computer time on a CRAY YMP and a CRAY C90 of the CRAY Research Park, MN, is also gratefully acknowledged.

REFERENCES

1. E. Lennemann, 'Aerodynamic aspects of disk files', *IBM J. Res. Dev.*, **18**, 480–488 (1974).
2. R. Kaneko, S. Oguchi and K. Hoshiya, 'Hydrodynamic characteristics in disk packs for magnetic storage', *Rev. Electron. Commun. Lab.*, **25**, 1325–1336 (1977).
3. S.D. Abrahamson, J.K. Eaton and D.J. Koga, 'The flow between shrouded corotating disks', *Phys. Fluids A*, **1**, 241–251 (1989).
4. C.A. Schuler, W. Usry, B. Weber, J.A.C. Humphrey and R. Greif, 'On the flow in the unobstructed space between shrouded corotating disks', *Phys. Fluids A*, **2**, 1760–1770 (1990).
5. H.M. Tzeng and J.A.C. Humphrey 'Corotating disk flow in an axisymmetric enclosure with and without a bluffbody', *Int. J. Heat Fluid Flow*, **12**, 194–201 (1991).
6. J.A.C. Humphrey, C.A. Schuler and D.R. Webster, 'Unsteady laminar flow between a pair of disks corotating in a fixed cylindrical enclosure', *Phys. Fluids A*, **7**, 1225–1240 (1995).
7. J.A.C. Humphrey and D. Gor, 'Experimental observations of an unsteady detached shear layer in enclosed corotating disk flow', *Phys. Fluids A*, **5**, 2438–2442 (1993).
8. J.A.C. Humphrey, C.A. Schuler and I. Iglesias, 'Analysis of viscous dissipation in disk storage systems and similar flow configurations', *Phys. Fluids A*, **4**, 1415–1427 (1992).
9. C.J. Chang, C.A. Schuler, J.A.C. Humphrey and R. Greif, 'Flow and heat transfer in the space between two corotating disks in an axisymmetric enclosure', *J. Heat Transfer*, **111**, 625–632 (1989).
10. H.M. Tzeng and J.E. Fromm, 'Airflow study in a cylindrical enclosure containing multiple corotating disks', *IBM Research Report RJ7334*, IBM, 1990.
11. C.J. Chang, J.A.C. Humphrey and R. Greif, 'Calculation of turbulent convection between corotating disks in axisymmetric enclosures', *Int. J. Heat Mass Transfer*, **33**, 2701–2720 (1990).
12. W.H. Finlay, J.B. Keller and J.H. Ferziger, 'Instability and transition in curved channel flow,' *J. Fluid Mech.*, **194**, 417 (1988).
13. I. Iglesias, 'Numerical investigation of the flow between a pair of disks corotating in a cylindrical enclosure', *Ph.D. Thesis*, Department of Mechanical Engineering, University of California at Berkeley, 1994.
14. B.P. Leonard, 'Stable and accurate convective modeling procedure based on quadratic upstream interpolation', *Comput. Methods Appl. Mech. Eng.*, **19**, 59–98 (1979).
15. A.J. Chorin, 'A numerical method for solving incompressible viscous flow problems', *J. Comput. Phys.*, **2**, 12–16 (1967).
16. B.F. Blackwell and B.F. Armaly, 'Benchmark problem definition and summary of computational results for mixed convection over a backward facing step', *Computational Aspects of Heat Transfer-Benchmark Problems*, New Orleans, LA, ASME Winter Annual Meeting, 1–10, 1993.
17. I. Iglesias, J.A.C. Humphrey and F. Giralt, 'Numerical Calculation of Two Dimensional, Buoyancy-Assisted Flow Past a Backward Facing Step in a Vertical Channel', in B.F. Blackwell and B.F. Armaly (eds.), *Computational Aspects of Heat Transfer-Benchmark Problems*, ASME, New York, 1993, HTD-Vol. **258**, pp. 63–72.

18. A.Z. Szeri, S.J. Schneider, F. Labbe and H.N. Kaulman, 'Flow between rotating disks; Part I, basic flow', *J. Fluid Mech.*, **134**, 103–131 (1983).
19. S.J. Tavener, T. Mullin and K.A. Cliffe, 'Novel bifurcation phenomena in a rotating annulus', *J. Fluid Mech.*, **229**, 483–497 (1991).
20. C.A. Schuler, 'Investigation of the flow between rotating disks in an enclosure', *Ph.D. Thesis*, Department of Mechanical Engineering, University of California at Berkeley, 1990 .

